3D Printer Nozzle Can Be Hot and Stressed

ME123 Autumn 2020, Stanford University

Rio Hall-Zazueta, Ian Hong, Hansub Kim, Cole Maxwell

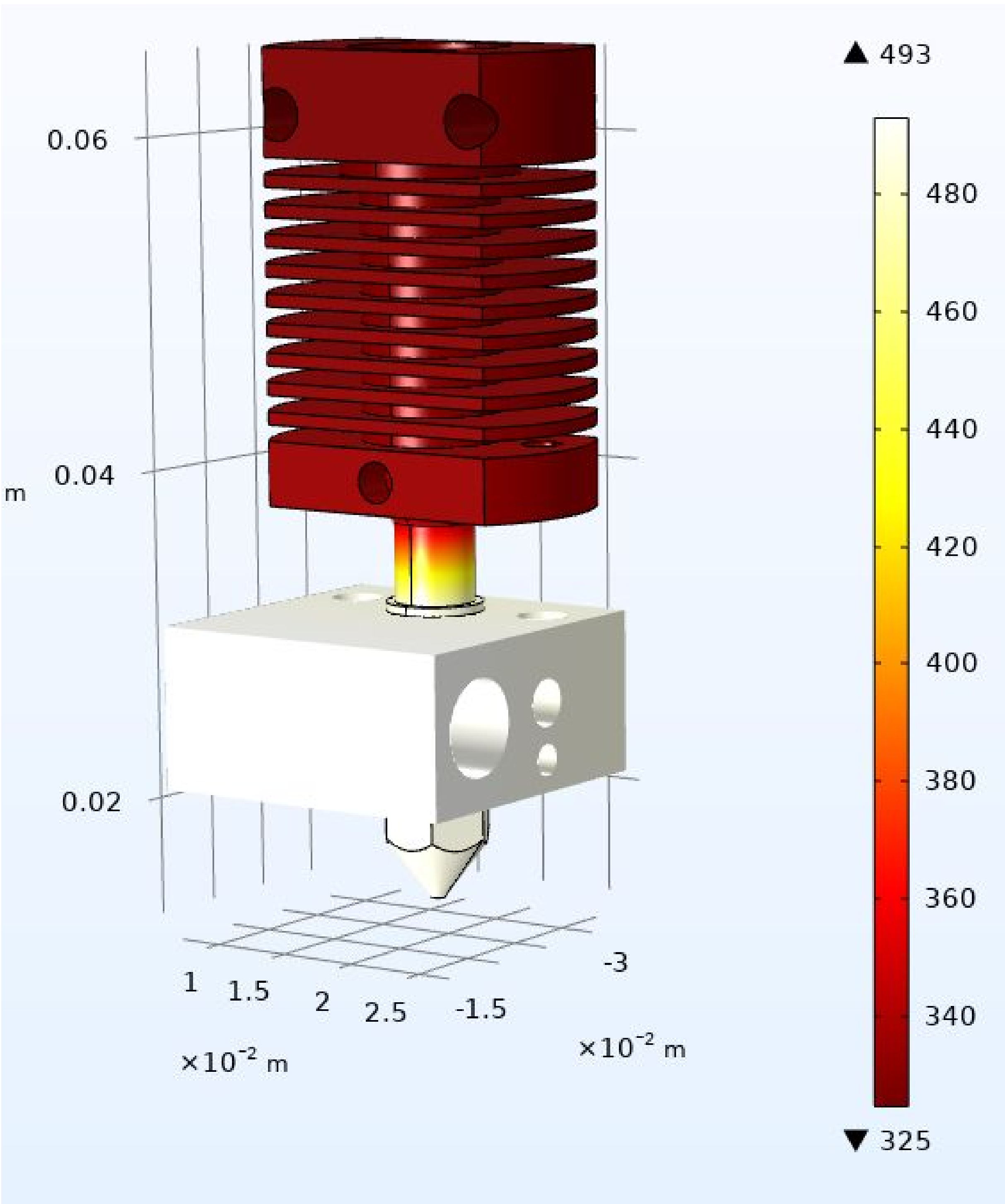

Abstract: This research paper discusses the simulation of the Ender 3 3D printer in COMSOL Multiphysics. The extruder components, specifically the nozzle, heat block, heat break, and radiator, were simulated using 3D geometry.

A coupled study was run on the modeled geometry to investigate air cooling coefficient approximation and thermal stress generation. Results were validated using experimental data as well as mesh refinement.

1. Introduction

The sophistication of 3D printers continues to evolve at a rapid rate, making them increasingly useful in manufacturing processes. Furthermore, true to their origins, 3D printers remain a valuable tool for designing, prototyping, and teaching [1]. The Stanford Mechanical Engineering department has taken full advantage of this tool in classes such as ME 102 and 103.

Figure 1. Creality Ender 3 3D Printer [2]

As part of its efforts to adapt to virtual teaching, Stanford has launched a program called P3D, which sends Ender 3 Fused Deposition Modeling 3D printers (pictured in Figure 1) to students enrolled in product realization classes. 3D printers create a unique compromise between accessibility, speed, cost, and precision, making them ideal for filling the gaps in virtual classes dealing with manufacturing techniques. All team members received 3D printers through this program.

As FDM 3D printing requires the careful management of high-temperature components, it is crucial to understand how heat moves between components and what stresses result. In pursuit of this objective, this study simulates heat transfer and thermal stress in the extrusion components of the 3D printer. The analysis is loosely modeled on the work of Thomas Hofstaetter et al. in the paper “Simulation of a Downsized FDM Nozzle” [3].

The first objective of this study was to approximate fan airflow over the heatsink without modeling fluid flow. The results from this first part were used to create a heat profile for the extrusion components. As a secondary multiphysics component of the study, thermal stress in the nozzle during heating was simulated and analyzed to gain insight into how and why it might deform or otherwise perform worse over time, which is important because nozzle issues are some of the most frequently encountered problems during printing [4]. This paper lays the groundwork for computationally accessible simulation of the extrusion components.

For result validation for the heat transfer study, the team members conducted timed studies of their 3D printers to obtain the expected heating time. To verify the thermal stress results, mesh refinement was performed.

2. Methods

The simulation was performed using COMSOL, a multiphysics modeling and simulation software. The model used for this study contained the entire sprinkler/extruder assembly, including parts for thermal management. The physics solvers used in this study were:

- Heat Transfer (solids)
- Solid Mechanics (solids)

2.1 Modeling and Meshing

The model used in this study was assembled directly from the official open-source CAD models of the Ender 3 printer on GitHub [5]. The specific parts used were:

- An aluminum radiator
- An aluminum heater block
- A steel heat break
- A brass nozzle

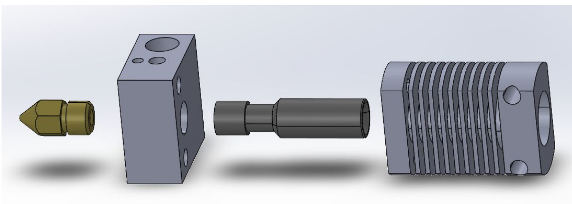

Figure 2. Left to right: Exploded CAD assembly of the nozzle, heater block, heat break, and radiator

Using Solidworks, the parts were combined into a single assembly as shown in Figure 2 (exploded view). The threading on the catheter was removed in Solidworks to provide a more accurate interface between the catheter and the heat block. Mates were slightly adjusted from their standard positions to ensure proper contact between parts.

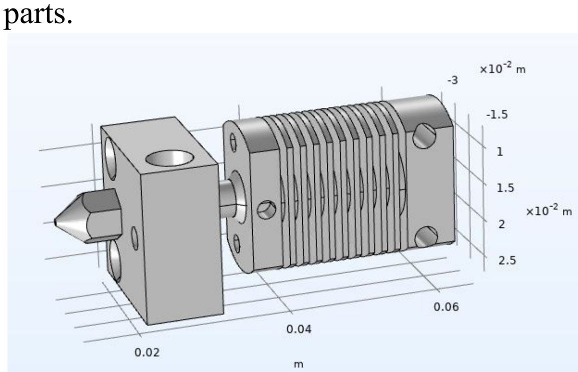

Figure 3. Processed Geometry in COMSOL

This assembly was then imported into COMSOL as a 3D geometry as shown in Figure 3. The assembly was meshed using a triangular normal size physics-controlled mesh, and materials were assigned to the components as defined earlier. The brass nozzle uses a custom material with parameters specified using brass averages [6].

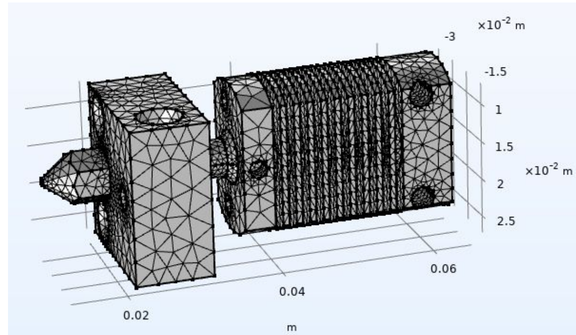

Figure 4. Meshed Geometry in COMSOL

Of note is the fact that the mesh, pictured in Figure 4, contains a few areas where the mesh is slightly more concentrated. This is due to the complex interfaces between the components. While this geometry is not ideal for meshing, it is the most accurate representation of the extrusion assembly.

2.2 Heat Transfer

Objective: The objective of the first part of the COMSOL analysis was to determine the heat transfer coefficient which best simulated fan airflow (forced convection cooling) across the hot end assembly. This value was identified by performing a time-controlled, heat transfer study of the hot end as it powered from room to operating temperature while testing several heat transfer coefficients using a parametric sweep. The appropriate value was determined by comparing the COMSOL results with the time it takes for the nozzle to experimentally reach operating temperature. The heat transfer coefficient which best approximated the experimental time was selected from the resulting data.

Physics: The Heat Transfer in Solids Module was used. The governing equations are as follow:

Heat Transfer Equation in Solids:

$$\rho C_p\left(\frac{\partial T}{\partial t} + u \cdot \nabla T\right) = \nabla \cdot (k\nabla T) + Q + Q_{ted}$$

Preliminary Results and Experiments: The operating temperature of the Ender 3D for PLA filament, 210℃, was found by referencing the user manual. The time it takes for the hot end to reach this temperature was determined experimentally.

Each member of the team measured the time it took for the nozzle to reach 210℃ over four trials, as well as the starting temperature of the nozzle. These results were used to calculate the average time for the hot end to heat up, 111.2(s). The average starting temperature of the nozzle, 296.7125(K), was also calculated and used as the ambient temperature in the initial conditions. To confirm that the results were within a reasonable statistical range the Z-score was calculated for each value. Since none of the trials had a Z-score of magnitude greater than three, none of the trials were excluded as outliers (Z-scores and full experimental data are in the appendix).

Initial Conditions: The Initial Conditions for the temperature of the assembly were that the components are at 296.7125(K). To simplify the analysis further, the following assumptions were made:

It was assumed that the heat transfer coefficient from forced convection cooling is constant over the surfaces specified in the BC section. A constant heat transfer coefficient represents an approximation of the average heat transfer over all affected surfaces, such that $h_{avg} = \frac{\int_S h(x)\cdot dx}{\int_S dx}$. This is a modeling choice as opposed to a physically accurate representation of the heat transfer coefficient at any specific point, which is determined by factors like geometry, boundary length, and flow velocity. The average heat transfer coefficient is still a useful metric. For example, the heat transfer coefficient along the length of the cylinder can be grossly approximated by this formula: $h(x) = \frac{h_{avg}}{2\sqrt{x}}$

No filament is present within the extrusion components. It has been previously determined that the presence of filament has little effect on heat flow in the model [3].

Ambient temperature remains constant at 23.5625℃.

Boundary Conditions: 4 types of boundary conditions were used to simulate heat flow in the hot end:

Shown in Figure 5, a constant boundary heat source of 40(W) was placed at the cylindrical surface where the heating cartridge is seated [9].

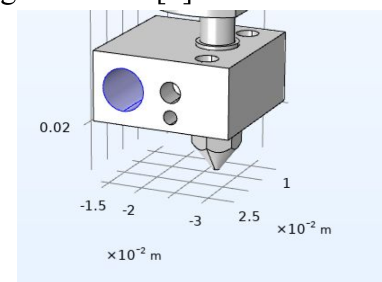

Figure 5. Boundary Heat Source

Shown in Figure 6, a convective heat flux condition was applied to the select surfaces of the radiator and the heat block to simulate forced convection cooling by the fan. The value of this heat coefficient was varied using a parametric sweep to find the appropriate value. However the value of the heat transfer coefficient was assumed to be constant for the heating process, since the fan runs at constant speed throughout the printer's operation [10].

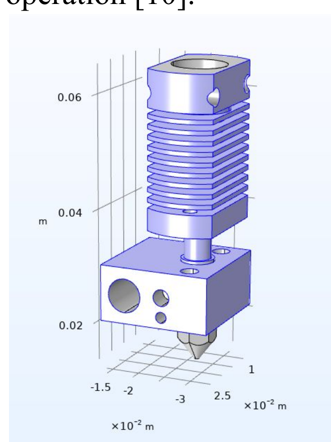

Figure 6. Forced Air Boundary Condition

Shown in Figure 7, a convective heat flux condition was applied to the surfaces of the nozzle and exposed surfaces not covered in the previous swept coefficient. The value of this coefficient remained constant at 15W/(m²K) to simulate convective cooling to still air [3].

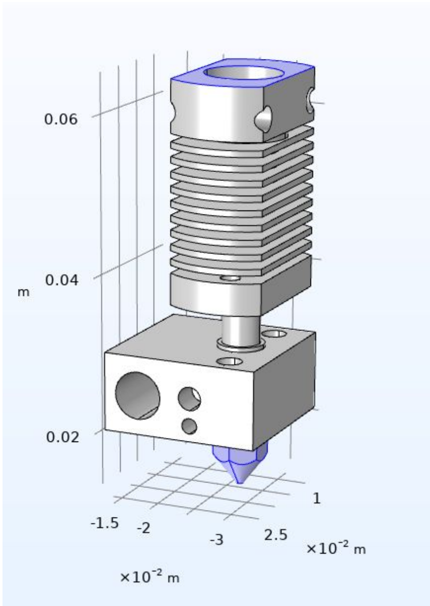

Figure 7. Still Air Boundary Condition

Shown in Figure 8, a thermally insulated boundary condition was applied to all remaining surfaces, including the top surface, the radiator, and the bottom surface of the heat sink. These surfaces border the hot end enclosure.

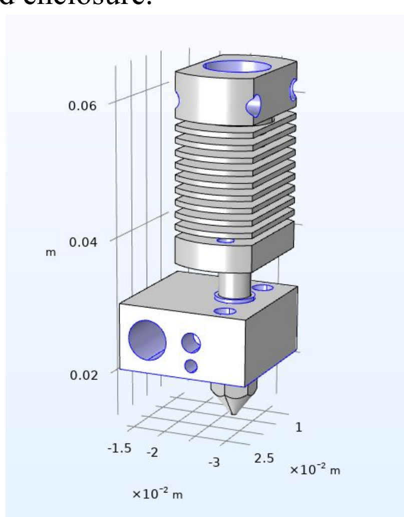

Figure 8. Thermally Insulated Boundary Condition

Study: A time-controlled study was evaluated from 0 to 111.4(s) at timestep of 0.2(s). The variable heat transfer coefficient was swept from 10 to 400W/(m²K) in increments of 20W/(m²K), and in secondary analysis from 15W/(m²K) to 20W/(m²K)in increments of 1W/(m²K).

Point Probes: One point probe was used in this portion of the analysis. The point probe was placed in the tip of the nozzle to mimic the location of the temperature sensor that records the nozzle temperature on the 3D printer. The probe expression was temperature (T).

2.3 Thermal Stress

Objective: The objective of this second part of our COMSOL analysis was to analyze the stresses created within the apparatus after it was heated to 210℃. Since the sprinkler assembly is composed of components made out of different materials that interact in complex ways, an analysis of the resulting thermal stresses would put a spotlight on potential areas of failure/weakness in the 3D printer.

The 3D temperature profile at t=111.2(s) was functionally transported into this segment of the study by using the final heat transfer coefficient from section 3.1 and running the same time dependent study. Since the 3D printer modulates the heating and cooling of the sprinkler once it has reached its target temperature, it was assumed that the temperature profile would be at a relatively steady state post-heating.

A 3D surface plot of Von Mises stresses was developed using the previous temperature profile, then individual point probes were placed at the locations of highest stress to determine the exact directions and magnitudes of the stresses.

Physics: This thermal stress analysis utilized a multiphysics study in COMSOL, combining Solid Mechanics and Heat Transfer in Solids to perform a Thermal Expansion analysis.

The governing equations are as follow:

Thermal Strain Equation: $\varepsilon = \alpha_T (T - T_{ref})$

Strain-Displacement Equation:
$\varepsilon_{ij} = \frac{1}{2}(u_{j,i} + u_{i,j})$
Hooke's Law: $\sigma_{ij} = C_{ijkl}\varepsilon_{kl}$

Initial Conditions: As this segment of the analysis was a multiphysics study, the initial conditions were separated into the Solid Mechanics ICs and Heat Transfer in Solids ICs:

For Solid Mechanics, the initial conditions were no initial displacements, velocities, or acceleration on any of the parts. Gravity here was assumed to be negligible.

For Heat Transfer in Solids, the initial conditions are the same as in section 2.2: all components start at room temperature, 296.7125(K).

Boundary Conditions: Like the initial conditions, the boundary conditions in this part of the study are separated into two parts.

For Solid Mechanics, the boundary conditions are free everywhere except the bolt holes that affix the assembly to the rest of the 3D printer, depicted in Figure 9 by the blue boundaries. This mirrors the actual setup of the sprinkler within its housing.

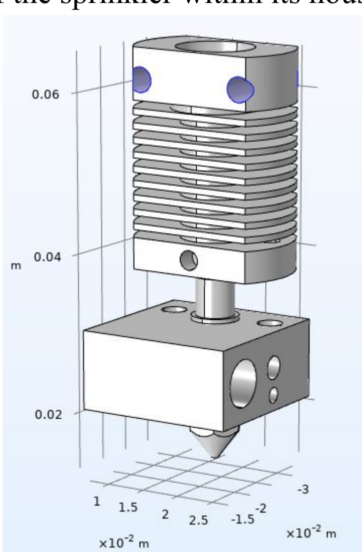

Figure 9. Fixed Boundary Condition

For Heat Transfer in Solids, the boundary conditions are identical, with the removal of the parametric sweep over the forced convective cooling coefficient. This was replaced with the static coefficient determined in section 2.2 of 18.7W/(m²K).

Study: The analysis was performed using a time-dependent study that ran from 0s to 111.2(s) in 0.2(s) increments. This end time was selected based on experimental heating data.

Point Probes: Point probe locations were determined based on areas of interest in the surface Von Mises stress plot; exact locations are discussed in section 3.4. Each probe had four separate expressions: Von Mises Stress (solid.mises), Tensile Stress (solid.sp1), Compressive Stress (solid.sp3), and 2nd Principal Stress (solid.sp2). Note that Compressive Stress is reported on a reverse scale, with negative values indicating larger compressive stress. The focus in this study was on the tensile and compressive stresses due to the nature of the assembly. The 2nd Principal Stress was included primarily to support mesh refinement validation, and was not used as part of the analysis or considered in the discussion [7]. Results were taken at t = 111.2(s) to approximate heated behavior.

3. Results and Discussion

The analyses described above were performed in pairs by the group members. Cole and Rio handled the Heat Transfer study and analysis, and Hansub and Ian took charge of the Thermal Stress experiment and interpretation.

3.1 Heat Transfer Results

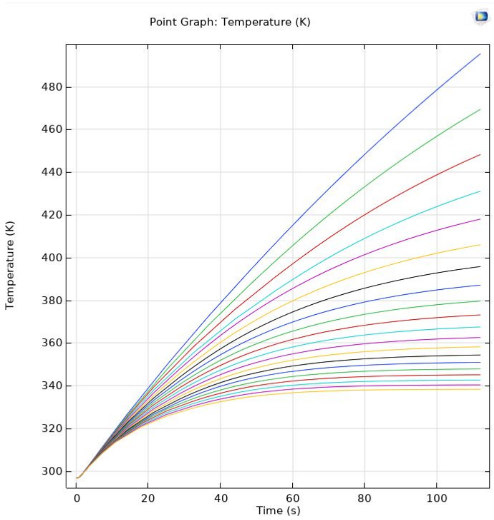

Figure 10. Temperature (K) vs. Time (s) - Parametric Sweep 1 of Heat Transfer coefficient

The results of the parametric sweep are shown in Figure 10, which displays the coarse parametric sweep temperature rise over time at the probe point on the nozzle. This first parametric sweep was used to determine the general bounds for acceptable heat transfer coefficients.

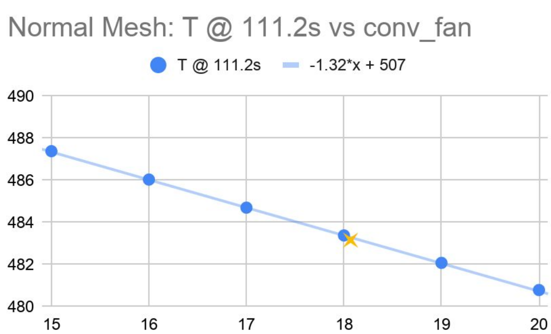

Figure 11. Temperature (K) at 111.2(s) vs. Heat Transfer coefficient (W/m^{2}K) - Parametric Sweep 2

Using the data gathered in the prior parametric sweep, a second sweep was run from 15W/(m²K) to 20W/(m²K), using increments of 1W/(m²K). The resulting data is shown in Figure 11. A linear extrapolation was then used to calculate the coefficient for which the nozzle point probe reached 483.15(K) at 111.2(s), to match the experimental data.

3.2 Heat Transfer Validation

To validate the Heat Transfer results, a mesh refinement study was performed. The same parametric sweep performed above for the normal mesh was performed for fine, finer, and extra fine meshes. The normal mesh has 45,570 elements. The fine mesh has 74,397 elements. The finer mesh has 135,788 elements. The extra fine mesh has 326,720 elements.

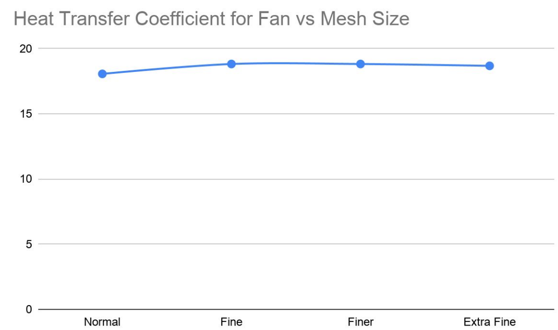

Figure 12. Heat Transfer coefficient (W/m^{2}K) vs. Mesh Size

The results of the mesh refinement study are shown in Figure 12. The coefficients found for these four different mesh sizes are all within acceptable bounds. The percent error from the average for the heat transfer coefficient decreases as the mesh is refined. The percent error is 2.86% for the normal mesh, 1.21% for the fine mesh, 1.21% for the finer mesh, and 0.45% for the extra fine mesh. All of these values remain under 5%. Using the scattered data points, the final determined heat transfer coefficient was adjusted to a value of 18.7W/(m²K). *See appendix for parametric sweep data for all meshes*.

3.3 Heat Transfer Discussion

The heat transfer coefficient value of 18.7 W/(m^{2}K) is given the initial and boundary conditions. The expression for the heat transfer coefficient is given by $h = Q/\Delta T$, where Q is the heat flux and T is the temperature differential between the outside fluid and solid surface. Given that the air temperature immediately surrounding the solid surface is an order of 10^1 smaller than the solid temperature, the heat transfer coefficient is within the line of reason for this setup.

Additionally, given the relatively small size of the 24(V) fan, it is reasonable that the heat transfer coefficient would not be significantly different from the 15W/(m^{2}K) heat transfer coefficient used to approximate still air. In future analysis, data might be collected by introducing the additional effect of the second fan. This fan primarily serves to blow on parts that have been printed, but the nozzle is also in the path of its expelled air. Accounting for this fan could help refine heat transfer data for and around the nozzle.

3.4 Thermal Stress Results

Using the previously mentioned conditions, the Thermal Expansion study was run.

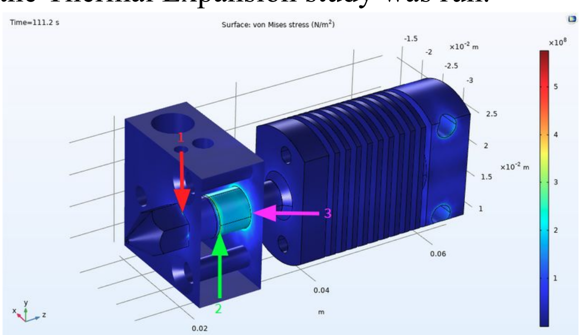

Figure 13. Surface Von Mises Stress (N/m^2)

The resulting surface Von Mises stress plot is shown in Figure 13, with one wall of the heat block hidden to show interior stresses. This plot was used to determine the areas of highest stress and most interest; Areas 1, 2, and 3 were chosen as follows:

Area 1 (red): Nozzle-Heat Block interface
Area 2 (green): Nozzle-Catheter interface
Area 3 (pink): Catheter-Heat Block interface

These areas of interest follow not only the simulated results, but also intuitive reasoning. In this part of the study, the primary contributing factor to thermal stress will likely be the unequal thermal expansion of components due to their different materials.

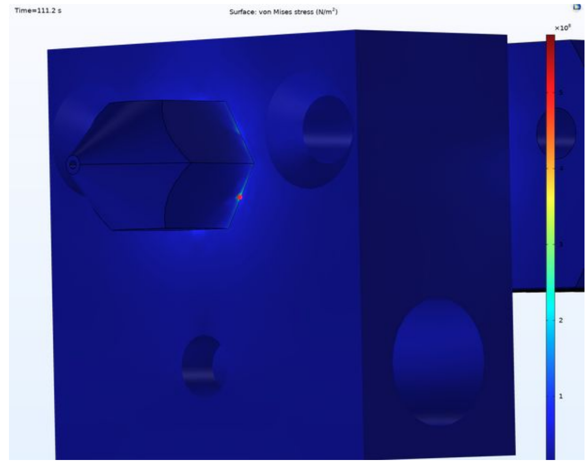

Figure 14. Point Probe 1

Area 1 was probed using boundary Point Probe 1, indicated by the red dot in Figure 14. This probe was located on the nozzle near its contact boundaries with the Heat Block.

Von Mises	Tensile	Compressive	2nd Principal
2.368E8	5.266E7	-2.186E8	-5.282E7

Table 1. Point Probe 1 Stresses (N/m^2)

The resulting stresses at this location are displayed in Table 1.

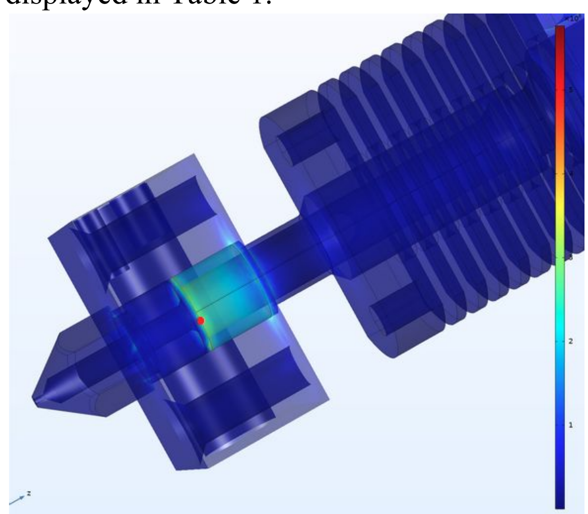

Figure 15. Point Probe 2

Area 2 was probed using Domain Point Probe 2 indicated by the red dot in Figure 15. This probe is located at the interface between the nozzle and the catheter.

Von Mises	Tensile	Compressive	2nd Principal
2.332E8	2.700E8	2.425E8	1.630E8

Table 2. Point Probe 2 Stresses (N/m^2)

The resulting stresses at this point are displayed in Table 2.

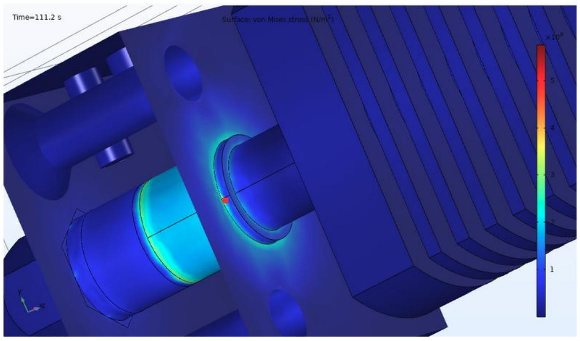

Figure 16. Point Probe 3

Area 3 was probed using Boundary Point Probe 3, indicated by the red dot in Figure 16. This probe was located on the outside diameter of the catheter near its boundary with the heat block.

Von Mises	Tensile	Compressive	2nd Principal
3.796E8	-6.567E7	-4.936E8	-1.974E8

Table 3. Point Probe 2 Stresses (N/m^2)

The resulting stresses at this location are displayed in Table 3.

3.5 Thermal Stress Validation

The Thermal Stress results were validated using a mesh refinement analysis. The normal-sized mesh had 45,570 elements, the fine-sized mesh had 74,397 elements, and the finer-sized mesh had 135,788 elements.

As indicated by the results in Figures 17, 18, and 19, there is little variation in stress as mesh size decreases.

In the context of this study, calculating specific stress values was less important than finding general stress directions and orders of magnitude at areas. so the fluctuations are not concerning.

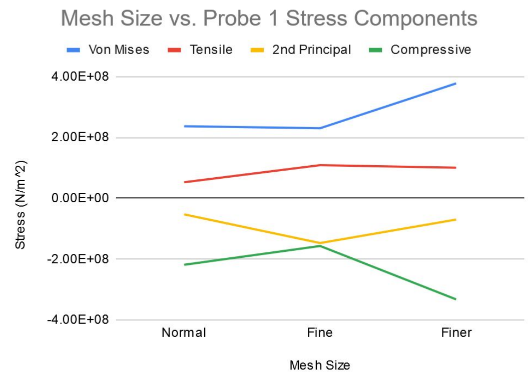

Figure 17. Point Probe 1 Mesh Refinement

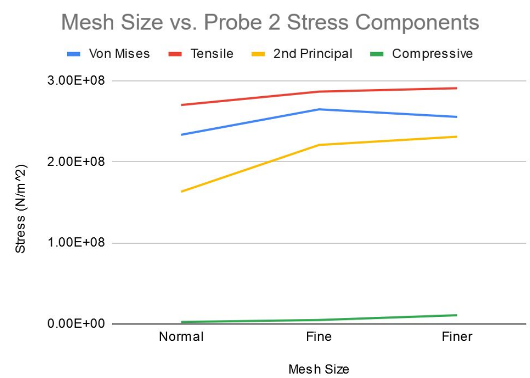

Figure 18. Point Probe 2 Mesh Refinement

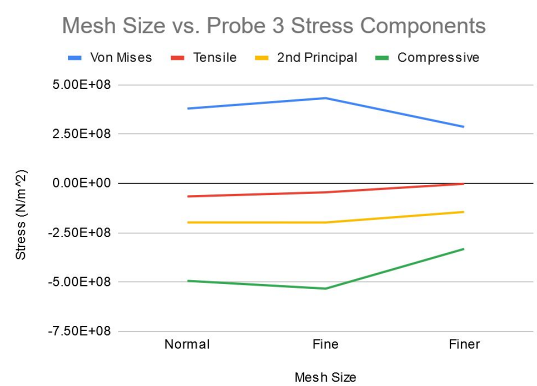

Figure 19. Point Probe 3 Mesh Refinement

The margins of error between the different mesh sizes can be largely explained by the model itself; variations in mesh sizing and element placing between studies likely contributed to the observed discrepancies, as probes were selected close to component boundaries. This analysis could be made more accurate by manually defining the mesh in order to get a proper result at each probe point for each mesh size.

While the results at Probes 1 and 3 indicate the possibility of a mesh singularity forming, this does not appear to be the case. Analyzing the mesh generated with the mesh set to ‘finer’, the following behaviors occur around the probe points’ locations, as shown in Figures 20 and 21:

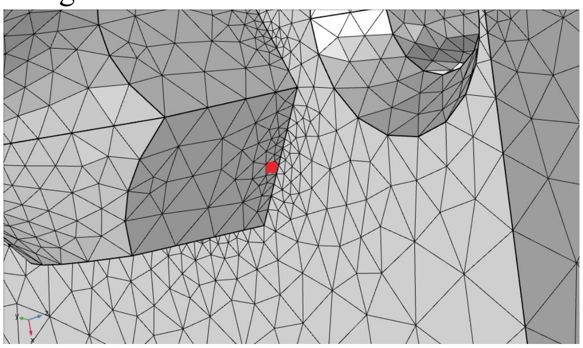

Figure 20. Point Probe 1 - Finer Mesh

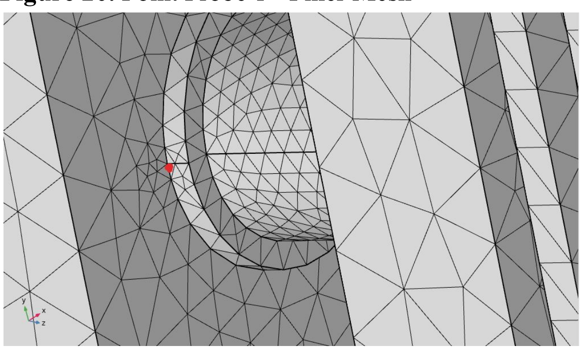

Figure 21. Point Probe 3 - Finer Mesh

A visual inspection of these areas does not appear to indicate the development of any singularities. Though the exact values of the stresses were not of concern in this study, this could be a possible point of improvement for the model, as future extensions could be more sensitive to exact mesh definitions.

3.6 Thermal Stress Discussion

Qualitatively, stresses in the areas of interest can be characterized as follows, using linear heat expansion coefficients [8].

Area 1 (Nozzle-Heat Block boundary): Exhibits largely compressive stresses from the unequal expansion of components. While aluminum has a higher linear thermal expansion coefficient than brass, indicating that the nozzle cutout should expand more than the nozzle, this does not appear to be the case. In order to understand why, we must consider a number of factors, including how the components displace, what their geometries are, and what their respective thermal expansion coefficients are.

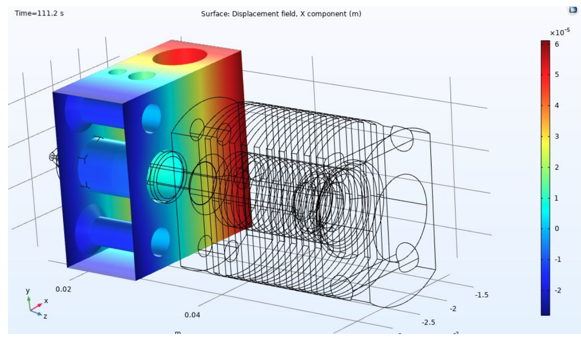

Figure 22. Heat Block X-Displacement (m)

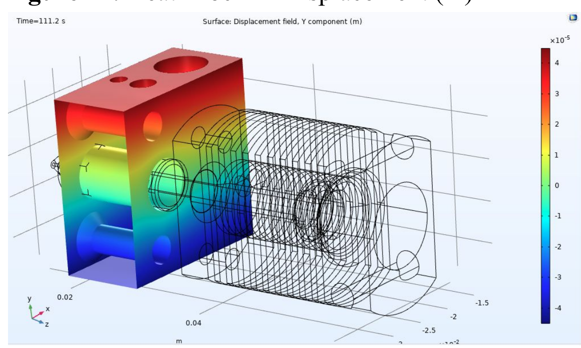

Figure 23. Heat Block Y-Displacement (m)

The displacement gradients in the heat block shown in Figures 22 and 23 indicate that the geometry of the heat block and location of the heating element have caused non uniform displacement, leading to compressive stresses along sections of the nozzle where the heat block has expanded less than the nozzle. It is also possible that these compressive stresses result from the unequal geometries of the heat block and nozzle having a larger effect on their expansion than their thermal expansion coefficients. The tensile stress exhibited in Point Probe 1 is likely due to mesh fragments being subjected to unequal and opposite forces, as thermal expansion of both the heat block and the nozzle force mesh nodes on either component to "stretch". It is important to note that because the probe point was defined as a general point of interest and not at specific boundaries, tensile stress values can fluctuate significantly depending on which mesh fragment our chosen point corresponded to and the quality of the mesh.

Area 2 (Nozzle-Catheter Interface): The catheter's threaded contact with the heat block prevents z-movement and creates large internal tensile stresses. Despite the locked z-movement, the catheter will still expand in the z-direction, meaning that it will apply a force on the nozzle in the z-direction, adding to the compressive stress it experiences. This directional compressive stress will likely be borne by the connection attaching the nozzle to the heat block. This area also experiences the same compressive stresses caused by the displacement gradients discussed in Area 1.

Area 3 (Catheter-Heat Block Interface): This area's stresses are primarily characterized by the same stresses present in Area 1. Large compressive stresses here result from the displacement gradient discussed in Area 1. Tensile stress is present at this contact boundary for the same reasons as in Point Probe 1; vertical thermal expansion of the catheter or the top portion of the heat block are largely responsible.

4. Conclusion

The team was satisfied with the study as a whole. After working through numerous challenges and setbacks, the team ultimately accomplished the stated goals of creating a thermal modeling framework for the Ender 3, and using said framework to perform preliminary analysis as a proof of concept and a rudimentary stress study.

In terms of valuable lessons learned, one of the most educational aspects of the study was reverse engineering the thermal management system of the Ender 3. This required trawling various internet forums and making logical extrapolations for information that wasn't explicitly stated. This process of deconstructing the modeled 3D printer sprinkler assembly and reassembling it brought forward many foundational questions for the project around how the thermal management system functions and what assumptions and approximations could be made.

With 6 additional months, the team would do the following:

- Refine the thermal management system model by reaching out to the Ender 3's manufacturer, Creality, to fully define the specifics of how it functions
- Refine the mesh in all areas by manually determining possible 'hot spots' and adjusting the mesh to provide a more accurate result across the entire geometry
- Test the limits of the created framework through different types of analyses
- Expand our experimental data portfolio by conducting many more studies

There are many possible extensions of the study, and the team would love to explore them down the road. They include filament flow, which would add an intriguing laminar flow component; component heating and cooling with a regulated heating source; and thermal management optimization, running parametric studies on different aspects of the radiator geometry and dimensions.

5. Appendix

Collected data on printer heating and Z-scores: (Z-score is calculated for time to 210℃)

Printer ID	Start temp (℃)	Time to 210℃ (s)	Z-score
Rio	26	113.80	-0.4694715883
Rio	27	114.18	0.5386520841
Rio	27	113.65	0.4421634979
Rio	27	113.59	0.4312402617
Ian	21	115.60	0.7971686737
Ian	21	115.41	0.7625784258
Ian	21	114.89	0.6679103789
Ian	21	115.20	0.7243470992
Hansub	23	111.08	-0.02571511851
Hansub	23	111.49	0.04892699539
Hansub	23	112.56	0.2437247073
Hansub	23	113.85	0.4785742851
Cole	25	112.50	0.2328014711
Cole	23	101.30	-1.806202616
Cole	23	98.13	-2.383313594
Cole	23	102.31	-1.62232814
Average	23.5625	111.22	

Additional parametric sweep data across various meshes:

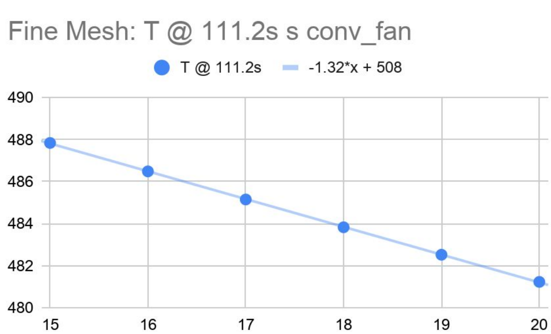

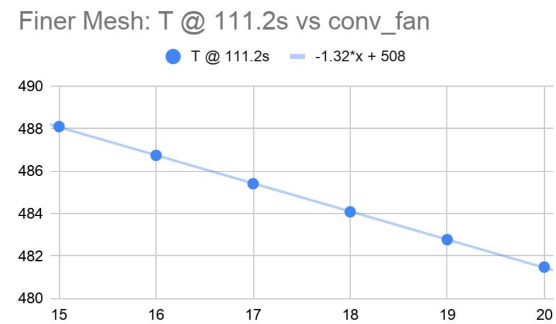

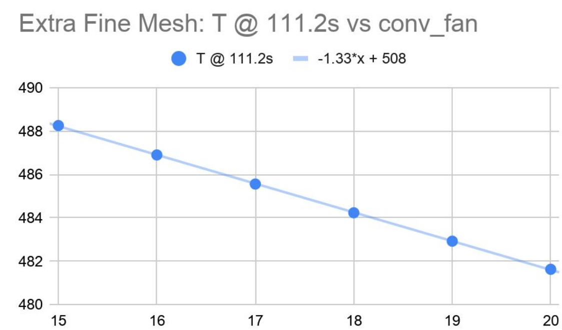

6. References

1. https://amfg.ai/industrial-applications-of-3d-printing-the-ultimate-guide/
2. https://images-na.ssl-images-amazon.com/images/I/51NYCnoa13L._SL1001_.jpg
3. https://www.researchgate.net/publication/292962364_Simulation_of_a_Downsized_FDM_Nozzle
4. https://all3dp.com/1/common-3d-printing-problems-troubleshooting-3d-printer-issues/
5. https://github.com/Creality3DPrinting/Ender-3/tree/master/Ender-3%20Mechanical/STP
6. http://www.matweb.com/search/datasheet_print.aspx?matguid=d3bd4617903543ada92f4c101c2a20e5
7. http://www.learneasy.info/MDME/MEMmods/MEM09155A-CAE/010-Intro-FEA/Intro-FEA.html
8. https://www.engineeringtoolbox.com/linear-expansion-coefficients-d_95.html
9. https://www.fargo3dprinting.com/products/ender-3-heater-cartridge/
10. https://images-na.ssl-images-amazon.com/images/I/D1N3oS2crrS.pdf